

One-dimensional edge state transport in a topological Kondo insulator

Yasuyuki Nakajima,¹ Paul Syers,¹ Xiangfeng Wang,¹ Renxiong Wang,¹ and Johnpierre Paglione^{1,*}

¹*Center for Nanophysics and Advanced Materials,
Department of Physics, University of Maryland, College Park, MD 20742*

GROWTH AND CHARACTERIZATION

Single crystals of SmB₆ were grown with Al flux, starting from pre-grown powdered SmB₆ (samples #1 and #2) and from elemental Sm and B with the stoichiometry of 1 to 6 (#3, #4, #5, and #6) in a ratio of SmB₆ : Al = 1 : 200 - 250. The starting materials were placed in an alumina crucible and sealed in a quartz ampoule or loaded in a tube furnace under Ar atmosphere. The whole assembly was heated to 1250 - 1400°C and maintained at that temperature for 70 - 120 hours, then cooled at -2°C/hr to 600 - 900°C, followed by faster cooling. After growth, some of batches were annealed at 1000 °C for 24 - 72 hours. The typical size of resulting crystals is $\sim 1 \times 1 \times 1$ mm³. The obtained samples were etched to remove the flux by hydrochloric acid or sodium hydroxide, sanded down by 400 grit paper and polished by 1000 grit one to clean the possible oxide layer or aluminum residues. Polished surfaces were shiny and smoothly flat.

We study the magnetotransport properties of slab-shape samples with different surface conduction, applying the electrical contacts by silver paint on one side of the samples. We also applied the contacts by spot-welding (written explicitly in the text, otherwise applied by silver paint). The resistance was measured with Lakeshore 370 AC resistance bridge. In Fig. S1, temperature dependence of sheet resistance $R_s = R \times w/l$ at zero field, where R is the measured 4 wire resistance, w and l are the width and distance between electrical contacts, is plotted for sample #1 corresponding to the sample shown in the main text (annealed, the thickness $t = 75$ μm , $w = 525$ μm , $l = 250$ μm) and #2 ($t = 40$ μm , $w = 450$ μm , $l = 250$ μm). Note that these samples are obtained from different batches. We apply the current along [100] direction of the cubic crystal structure. On decreasing T , R_s steeply increases below 10 K, showing insulating behavior, and the surface conductance dominates the charge transport below 3 K exhibiting saturation in the resistance. The inset of Fig. S1 shows the normalized resistance $R/R(300\text{ K})$ as a function of temperature for sample #1 and #2. At low temperatures, $R/R(300\text{K})$ of sample #2 is an order of magnitude smaller than that of #1, which indicates that the surface conduction of #2 is more dominant over the bulk conduction compared to #1.[1].

OSCILLATORY MAGNETORESISTANCE

We observe prominent oscillatory behavior in magnetoresistance (MR) in perpendicular field orientation ($I \parallel [100]$, $H \parallel [001]$) for the samples obtained from different batches, as shown in Figs. S2a and b. The amplitude of the oscillatory behavior decreases with temperature. By contrast, the oscillatory behavior is strongly reduced in the sweep-down MR shown in Figs. S2c and d compared to the sweep-up MR. In both samples, below 300 mK MR drops abruptly at very low fields on sweeping down field.

Assuming the oscillatory component is due to quantum oscillations gives us frequencies of 23 T for sample #1 and 17 T for #2 corresponding to the Fermi wave number $k_F = 0.26$ and 0.22 nm⁻¹, respectively. The obtained frequencies are close to the de-Haas van Alphen frequency for α pocket [2].

ANISOTROPY AND SHAPE OF HYSTERESIS

The observed hysteresis in MR shows strong anisotropy, depending on the field orientation to the surface with electrical contacts. In Figs. S3a and b, we display full "four quadrant" MR in perpendicular field orientation at 100 mK showing obvious hysteresis in MR of both samples below 10 T. The shape of the hysteresis strikingly differs from the shape of conventional ferromagnets, where the sweep-down MR is more conductive than the sweep-up and overshoots zero field. On the other hand, the hysteresis in parallel field orientation ($I \parallel [100]$, $H \parallel [010]$) plotted in Figs. S3c and d vanishes or becomes negligibly small. The strong anisotropy of hysteresis in magnitude of MR is responsible for the surface conduction.

The shape of hysteresis (Fig. S4) is quite inconsistent with the usual overshoot that requires to overcome a coercive field, but is indeed observed in certain situations, for instance, in exchange bias [3, 4] or 'negative' hysteresis [5] systems. In particular, the off-centered, symmetric shape of hysteresis in the magnetoresistance of SmB₆ is reminiscent of that of a randomly distributed exchange bias system, where the offset hysteretic loops originate from the intercoupling between a ferromagnetic layer and randomly oriented polycrystalline antiferromagnetic grains, yielding a rather exaggerated field response of magnetization as shown schematically in the

inset of Fig. S4 [6]. This situation would imply a field-polarized state above the hysteretic region, and thus the appearance of an anomalous Hall effect (AHE), and a magnetically ordered state at zero field. As discussed below, we do indeed observe an AHE component above the hysteretic range of magnetic field, consistent with this picture. However, considering the presence of a weak antilocalization (WAL) effect (see below) and lack of any anomaly in the temperature dependence of resistivity, the abrupt phase transition-like return of the MR to its virgin curve on down-sweep suggests that the zero-field surface state is paramagnetic and not long-range ordered, inconsistent with an exchange bias picture. It is worth considering a scenario where a similar random exchange bias interplay occurs between the surface ferromagnetism and bulk antiferromagnetic fluctuations or correlations, such as those observed by neutron scattering [7] and muon spin resonance experiments [8]. In any case, the nature of the magnetization must be directly experimentally verified before proceeding with any particular model as discussed here. More important, our conclusions about the role of ferromagnetic domain walls in yielding quantized conductance are not influenced by the details of the evolution of surface magnetism with field.

HYSTERESIS WITH DIFFERENT TURNING FIELDS

The turning field determines the shape of hysteresis in MR of SmB₆ as in ferromagnets. The hysteresis in MR of SmB₆ in perpendicular field orientation with different turning fields at 100 mK is shown in Figs. S4a and b. The hysteresis loop narrows with decreasing turning field less than 10 T, and the loop ends up disappearing below the turning field of 4T. Figures S4c and d show the difference between sweep-up and sweep-down magnetoconductance, $\Delta G = G_{up} - G_{down}$, obtained from the data shown in Figs. S4a and b. With decreasing the turning field, the peak of ΔG is strongly suppressed, and its position shifts to lower field.

ANOMALOUS HALL EFFECT

The Hall resistance R_{yx} is obtained by the antisymmetrization of the measured resistance R_{14} (R_{23}) between spot-welded transverse voltage probes V1 (V2) and V4 (V3) with $I \parallel [100]$ and $H \parallel [001]$ as shown in the inset of Fig. S5a, given by,

$$R_{yx}^{up}(H) = \frac{R^{up}(H) - R^{dn}(-H)}{2}, \tag{S1}$$

$$R_{yx}^{dn}(H) = \frac{R^{dn}(H) - R^{up}(-H)}{2}, \tag{S2}$$

where R^{up} (R^{dn}) is the up-(down-)sweep magnetoresistance. Note that the longitudinal resistance R_{xx} is symmetric with the following relation originating from the hysteretic behavior, $R_{xx}^{up}(H) = R_{xx}^{dn}(-H)$ and $R_{xx}^{dn}(H) = R_{xx}^{up}(-H)$ (Figs. S5a-d).

As shown in Figs. S6a-d, the anomalous Hall effect can be confirmed as a discernible kink around a closing field of ~ 8 T at 100mK, clearly exhibited in the difference of the Hall resistance $\Delta R_{yx} = R_{yx} - AH$ (the lower insets of Figs. S6a-d), where A is a linear coefficient obtained from fitting R_{yx} below 5 T, which strongly indicates the presence of surface ferromagnetic order. Although this ferromagnetic order induces the hysteresis in the longitudinal resistance, we observe no discernible hysteretic behavior in the Hall resistance, as shown in the deference between R_{yx}^{up} and R_{yx}^{dn} within our experimental resolution (the upper insets of Figs. S6b and d). The lack of observation of hysteresis in the Hall resistance can be attributed to substantial contribution from the massive Dirac surface states at the X/Y points, illustrated in Fig. 4d in the main text. Since the observed magnitude of Hall resistance is on the order of 0.1 Ω as shown in Fig. S6a-d, a rather sizable contribution of the massive surface states to the Hall conduction would easily mask a hysteretic component with magnitude of order $\sim e^2/h$.

DOMAIN WALL DYNAMICS

We observe domain wall dynamics in relaxation of MR. Figure S7 presents evidence of an asymmetric relaxation in the MR of SmB₆ sample #3 (contacts applied by spot welding) at 9 T between ascending and descending sweeps. The procedures to obtain the relaxation data are as follows: we fixed the base temperature (30 mK), and then, 1) for the ascending sweep, swept field up to 9 T, stopped, and measured the relaxation in the resistance as a function of time; 2) for the descending sweep, we swept field from 9 T up to 15 T, then down to 9 T, stopped, and measured the relaxation in the resistance. In both field sweeps, the sweep rate was 0.15T/min. As shown in Fig. S7, surprisingly, the relaxation after ascending sweep is much slower than that measured after descending sweep, although the sweep conditions in both the cases are identical. (It should be noted that the resistance change is not due to heating by eddy currents measured to be at most 1-2 mK – but mainly magnetoresistance.) This asymmetric relaxation between ascending and descending sweeps can be explained by domain wall dynamics in ferromagnetism. In the ascending sweep, majority domains develop with field along with minority domains and domain walls. The domain walls tend to move into an equilibrium state after stopping the sweep, showing a long relaxation time in the resistance. By contrast, in the descending sweep, all the domains are oriented with the large applied field, leading to no domain

walls, and therefore no dynamics and the absence of any measurable relaxation after stopping the sweep. This observation provides unequivocal evidence for the existence of ferromagnetic domains and domain walls that directly affect MR transport on the surface of our crystals.

NEARLY QUANTIZED MAGNETOCONDUCTANCE AND RANDOM RESISTOR NETWORK

The observation of nearly quantized magnetoconductance in several samples with different total absolute conductance values, surface quality and contact geometries and methods of contact preparation strongly suggests that the quantized magnetoconductance is intrinsic, not coincidental. We plot the difference of sweep-up and sweep-down magnetoconductance $\Delta G = G_{up} - G_{down}$ for sample #1 and #2 (contacts applied with silver paint), and #3 - #6 (spot-welded) as a function of magnetic field in Fig. S8. Surprisingly, in all the samples, ΔG shows a nearly quantized conductance of e^2/h at characteristic field $H^* \sim 5$ T. The observation of nearly quantized magnetoconductance can be attributed to a grid-shape domain structure forming a virtual infinite resistor network with conductance component $G = e^2/h$ in the presence of dissipation (Fig. 4c in the main text). The dissipation due to inelastic scattering at finite temperature and/or spatial variation of electronic structure, or "puddling" effect [9], virtually remove resistors at random from the infinite network, yielding the formation of a random resistor network with two conductance components of $G_1 = e^2/h$ and $G_2 = 0$, distributed randomly with the probability of p and that of $1-p$, respectively. Described by the percolating conduction theory [10], the equivalent conductance G_0 between any non-adjacent points in the random resistor network is $G_0 = (2p-1)G_1$ in the case of two dimensional system, consistent with the observed variation of nearly quantized magnetoconductance.

WEAK ANTILOCALIZATION

The observation of the WAL is one of the strong evidence for existence of the surface state. Figure S9a shows field dependence of sheet resistance R_s in parallel field orientation. We observe a sharp dip around zero field at low temperature. The dip becomes less prominent with temperature and vanishes at 400 mK, which is consistent with the signature of WAL. The WAL, destructive interference between time-reversed quasiparticle paths, is suppressed by magnetic field perpendicular to plane, as described by the Hikami-Larkin-Nagaoka (HLN) equation [11],

$$\Delta G_s = -\alpha e^2/2\pi^2\hbar[\ln(H_0/H) - \Psi(H_0/H + 1/2)], \quad (\text{S3})$$

where ΔG_s is a correction of sheet conductance, α is a WAL parameter, $\Psi(x)$ is the digamma function, $H_0 = \hbar/4eL_\phi^2$ and L_ϕ is the dephasing length.

However, the WAL is also observed in parallel field orientation, indicating the finite penetration depth λ of the surface states into bulk. In weak correlated topological insulators, such as Bi_2Se_3 , the penetration depth is negligibly small compared with the dephasing length [12]. By contrast, in SmB_6 , the penetration depth $\lambda \sim \hbar v_F/\Delta$, where Δ is the bulk gap size, can be longer due to the small gap size of $\Delta \sim 40$ K [13, 14]. Indeed, the long penetration depth in SmB_6 is consistent with an extremely high surface carrier concentration of $n_{2D} \sim 10^{14} \text{ cm}^{-2}$ observed in gating studies [1], in fact much higher than that of known confined electron systems [14]. Therefore a finite value of λ allows orbital motions of electrons even in H_{\parallel} field orientation, leading to a WAL correction in the sheet conductance given by,

$$\Delta G_s = -\alpha e^2/2\pi^2\hbar[\ln(1 + (H/H_{\parallel})^2)], \quad (\text{S4})$$

where $H_{\parallel} = \hbar/\sqrt{2}eL_\phi\lambda$ [15]. The extracted parameters for H_{\parallel} (Fig. 3d in the main text) yield a penetration depth of $\lambda = 142$ nm, which is indeed much larger than in weakly correlated TIs and comparable to the dephasing length.

We display the sheet conductance at low fields given by $\Delta G_s = G_s(H) - G_s(0)$ in Fig. S9b, and fit the data to the in plane WAL formula to extract α , L_ϕ , and λ . Using $L_\phi = 1.2\mu\text{m}$ at 20 mK obtained from fitting perpendicular field data to the HLN formula, we extracted $\lambda = 142$ nm. Obtained α is 0.29, which is much smaller than the expected $\alpha = 1/2 \times 2 = 1$ from top and bottom surface channels per Dirac cone. We show the temperature dependence of L_ϕ extracted from the fitting assuming temperature independent λ in Fig. S9c. L_ϕ varies as $T \propto T^{-0.5}$ attributed to electron-electron scattering in two-dimensional system at low temperatures, very similar to Ref.16. However, L_ϕ starts deviating from $T^{-0.5}$ dependence as approaching λ , suggesting breakdown of two dimensional analysis of the WAL ($L_\phi \sim \lambda$).

POSITIVE MAGNETORESISTANCE

We comment on positive MR observed in several reports [16, 17]. According to Ref. 16, orbital motion of the surface Dirac electrons under magnetic field gives rise to linear positive MR. The recent photo emission [18] and angular MR [17] studies suggest the existence of a topologically trivial surface channel with peculiar anisotropy showing two fold symmetry [17], and the surface channel strongly depends on a surface treatment. The positive MR with two fold symmetry in Ref. 16 could be responsible for the trivial channel. Actually, we observe positive MR with hysteresis in several samples. Typical

MR data taken for SmB₆ sample #4 with electrical contacts applied by spot-welding is shown in Figs. S10a and b, showing strong anisotropy of not only positive MR and hysteresis. Note that both perpendicular and parallel field data is taken without reapplying contacts. Although we took data without reapplying contacts, slight discrepancy in the resistance at 0 T is observed, indicating a thermal cycle causes modulation of the current path and/or a subtle change of surface states. Observation of positive MR with (our data) and without (Ref. 16) hysteresis indicates that the positive MR has nothing to do with chiral transport due to FM domain walls, supporting the presence of a trivial conduction channel.

We also observe strong anisotropy of weak antilocalization in SmB₆ sample #4 without reapplying electrical contacts (spot-welded) as shown in Figs. S10c and d. Using Eqs. 1 and 2, we extracted $\alpha_{\perp}=0.30$ for perpendicular and $\alpha_{\parallel}=0.49$ for parallel field orientation. The extracted penetration depth $\lambda = 161$ nm is comparable to #1 since λ is an intrinsic parameter.

* Electronic address: paglione@umd.edu

- [1] Syers, P., Kim, D., Fuhrer, M. S. & Paglione, J. Tuning Bulk and Surface Conduction in the Proposed Topological Kondo Insulator SmB₆. *Phys. Rev. Lett.* **114**, 096601 (2015).
- [2] Li, G. *et al.* Two-dimensional Fermi surfaces in Kondo insulator SmB₆. *Science* **346**, 1208–1212 (2014).
- [3] Giri, S., Patra, M. & Majumdar, S. Exchange bias effect in alloys and compounds. *Journal of Physics: Condensed Matter* **23**, 073201 (2011).
- [4] McCord, J. & Schäfer, R. Domain wall asymmetries in Ni₈₁Fe₁₉/NiO: proof of variable anisotropies in exchange bias systems. *New J. Phys.* **11**, 083016 (2009).
- [5] Esho, S. Anomalous Magneto-optical Hysteresis Loops of Sputtered Gd-Co Films. *Japanese Journal of Applied Physics* **15S1**, 93–100 (1976).
- [6] Zhao, T., Fujiwara, H., Zhang, K., Hou, C. & Kai, T. Enhanced uniaxial anisotropy and two-step magnetization process along the hard axis of polycrystalline NiFe/NiO bilayers. *Phys. Rev. B* **65**, 014431 (2001).
- [7] Fuhrman, W. T. *et al.* Interaction Driven Subgap Spin Exciton in the Kondo Insulator SmB₆. *Phys. Rev. Lett.* **114**, 036401 (2015).
- [8] Biswas, P. K. *et al.* Low-temperature magnetic fluctuations in the Kondo insulator SmB₆. *Phys. Rev. B* **89**, 161107 (2014).
- [9] Martin, J. *et al.* Observation of electron-hole puddles in graphene using a scanning single-electron transistor. *Nat. Phys.* **4**, 144–148 (2008).
- [10] Kirkpatrick, S. Percolation and Conduction. *Rev. Mod. Phys.* **45**, 574–588 (1973).
- [11] Hikami, S., Larkin, A. I. & Nagaoka, Y. Spin-Orbit Interaction and Magnetoresistance in the Two Dimensional Random System. *Prog. Theor. Phys.* **63**, 707–710 (1980).
- [12] Zhang, Y. *et al.* Crossover of the three-dimensional topological insulator Bi₂Se₃ to the two-dimensional limit. *Nat. Phys.* **6**, 584–588 (2010).
- [13] Cooley, J. C., Aronson, M. C., Fisk, Z. & Canfield, P. C. SmB₆: Kondo Insulator or Exotic Metal? *Phys. Rev. Lett.* **74**, 1629–1632 (1995).
- [14] Wolgast, S. *et al.* Low-temperature surface conduction in the Kondo insulator SmB₆. *Phys. Rev. B* **88**, 180405 (2013).
- [15] Tkachov, G. & Hankiewicz, E. M. Weak antilocalization in HgTe quantum wells and topological surface states: Massive versus massless Dirac fermions. *Phys. Rev. B* **84**, 035444 (2011).
- [16] Thomas, S. *et al.* Weak Antilocalization and Linear Magnetoresistance in The Surface State of SmB₆. *arXiv:1307.4133* (2013).
- [17] Chen, F. *et al.* Angular dependent magnetoresistance evidence for robust surface state in Kondo insulator SmB₆. *arXiv:1309.2378* (2013).
- [18] Zhu, Z.-H. *et al.* Polarity-Driven Surface Metallicity in SmB₆. *Phys. Rev. Lett.* **111**, 216402 (2013).

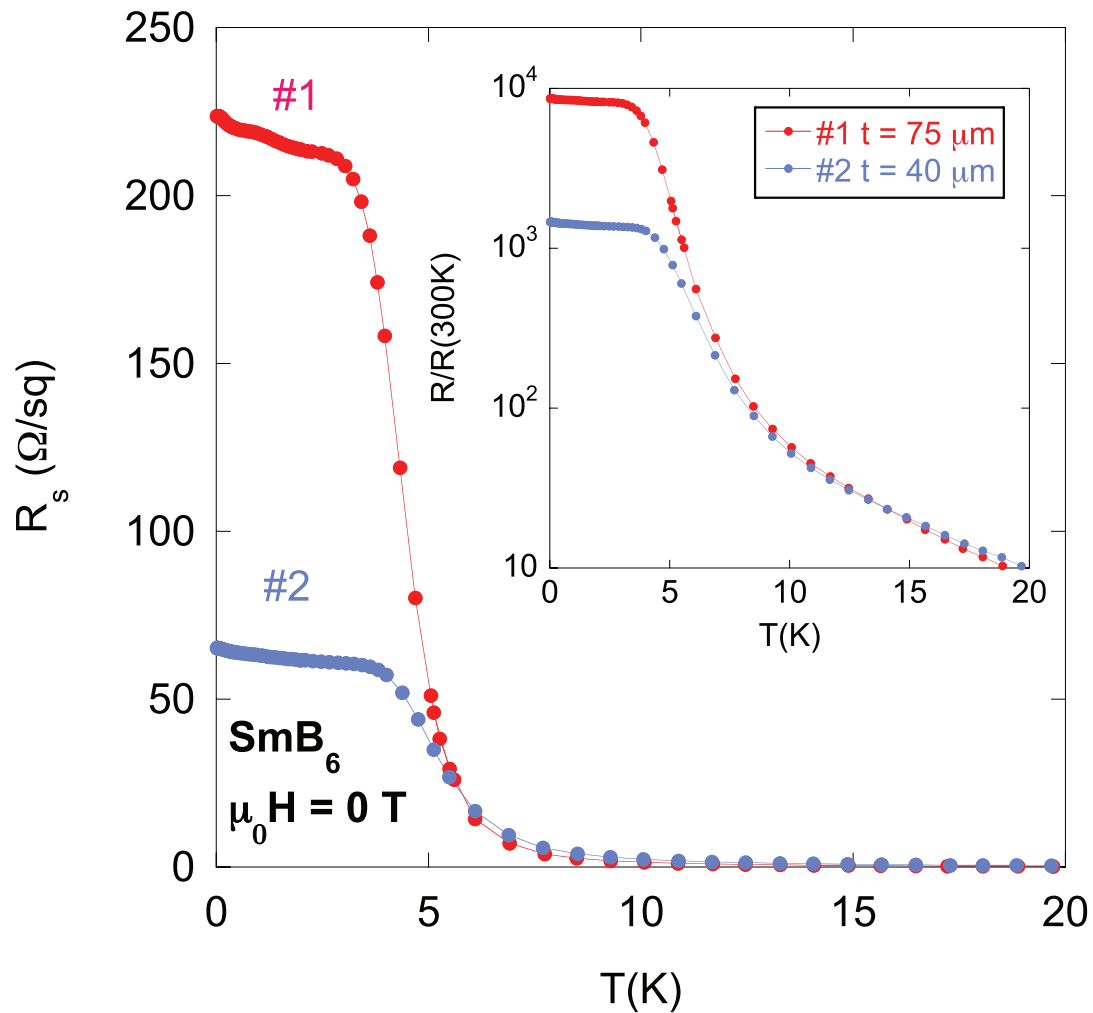


Figure S1: **Surface conduction in two different samples of SmB_6 .** Main panel: Temperature dependence of the sheet resistance R_s for sample #1 (the thicker sample with the thickness $t = 75 \mu\text{m}$) and #2 (the thinner sample with $t = 40 \mu\text{m}$) of SmB_6 . Inset: Normalized resistance $R/R(300\text{K})$ versus temperature for #1 and #2. At low temperatures, $R/R(300\text{K})$ of #2 is much smaller by an order of magnitude compared to #1, indicating the surface conduction of #2 is more dominant.

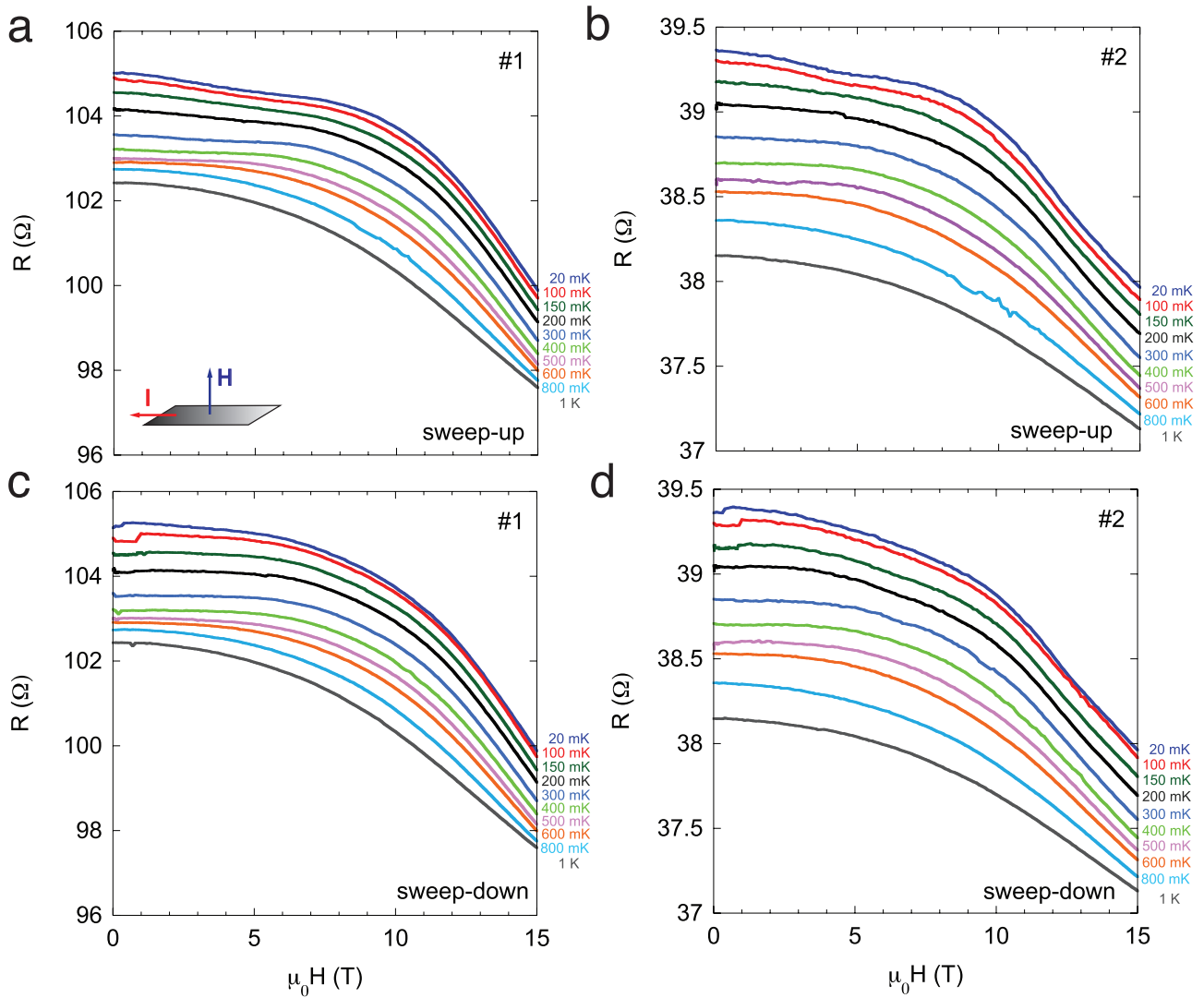


Figure S2: **Magnetoresistance in perpendicular field orientation of two different samples at low temperatures.** **a, b,** Sweep-up magnetoresistance in perpendicular field orientation ($I \parallel [100]$, $H \parallel [001]$) for #1 and #2. In both samples, oscillatory behavior is observed at low temperatures, and vanishes above 500 mK. **c, d,** Sweep-down magnetoresistance in perpendicular field orientation for #1 and #2. The oscillatory behavior observed in sweep-up magnetoresistance is strongly suppressed. Below 200 mK, we observe a sudden drop in magnetoresistance at low field.

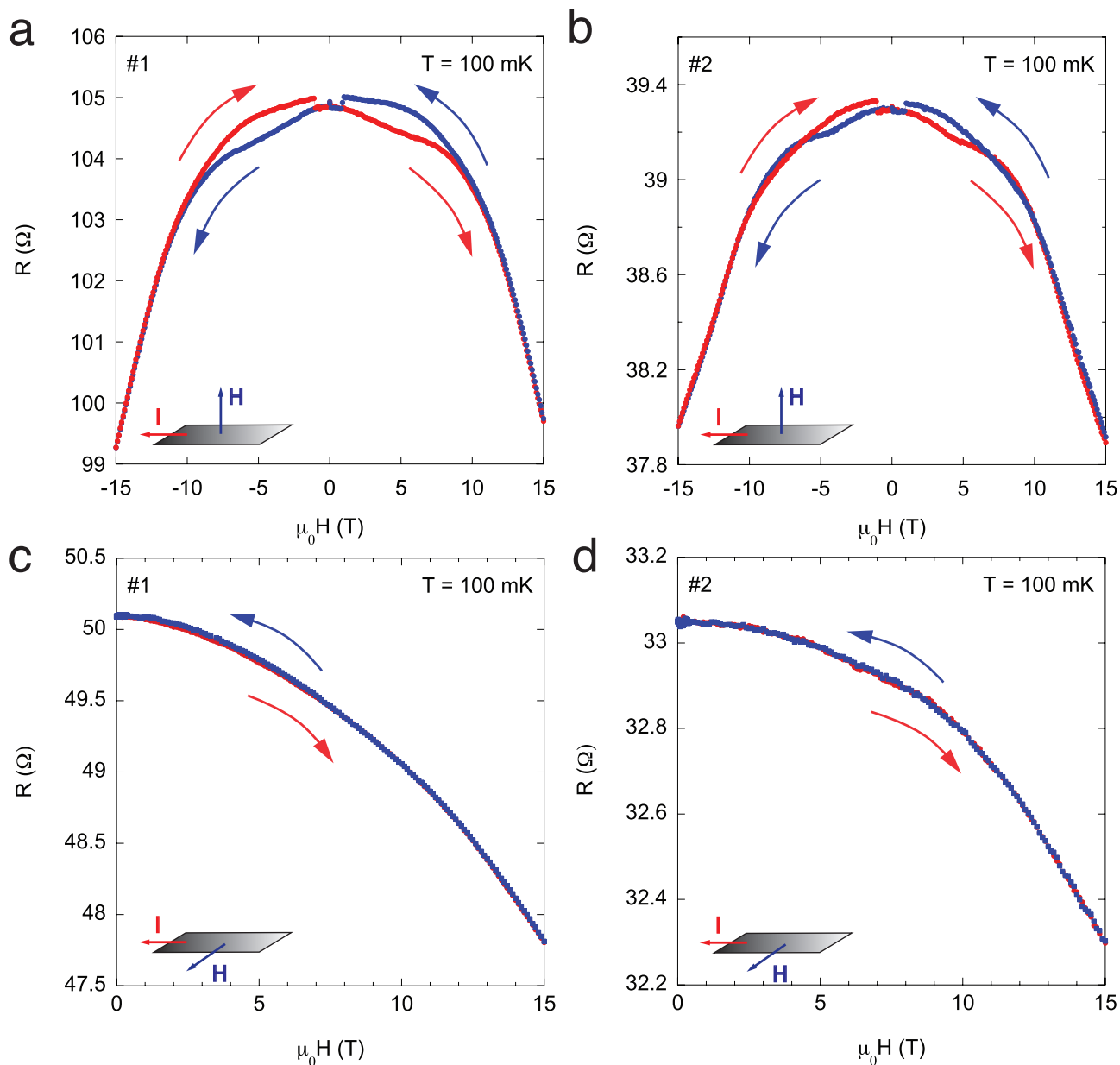


Figure S3: **Strong anisotropy of hysteresis in magnetoresistance.** **a, b**, Full "four quadrant" hysteresis loop in field perpendicular orientation ($I \parallel [100]$, $H \parallel [001]$) for sample #1 and #2 at 100 mK. We observe a butterfly shape but sign-reversal hysteresis in contrast to conventional ferromagnetic materials. **c**, Hysteresis loop in field parallel orientation ($I \parallel [100]$, $H \parallel [010]$) for sample #1 and #2 (with contacts reapplied) at 100 mK. The hysteresis observed in field perpendicular orientation is strongly suppressed, showing strong anisotropy.

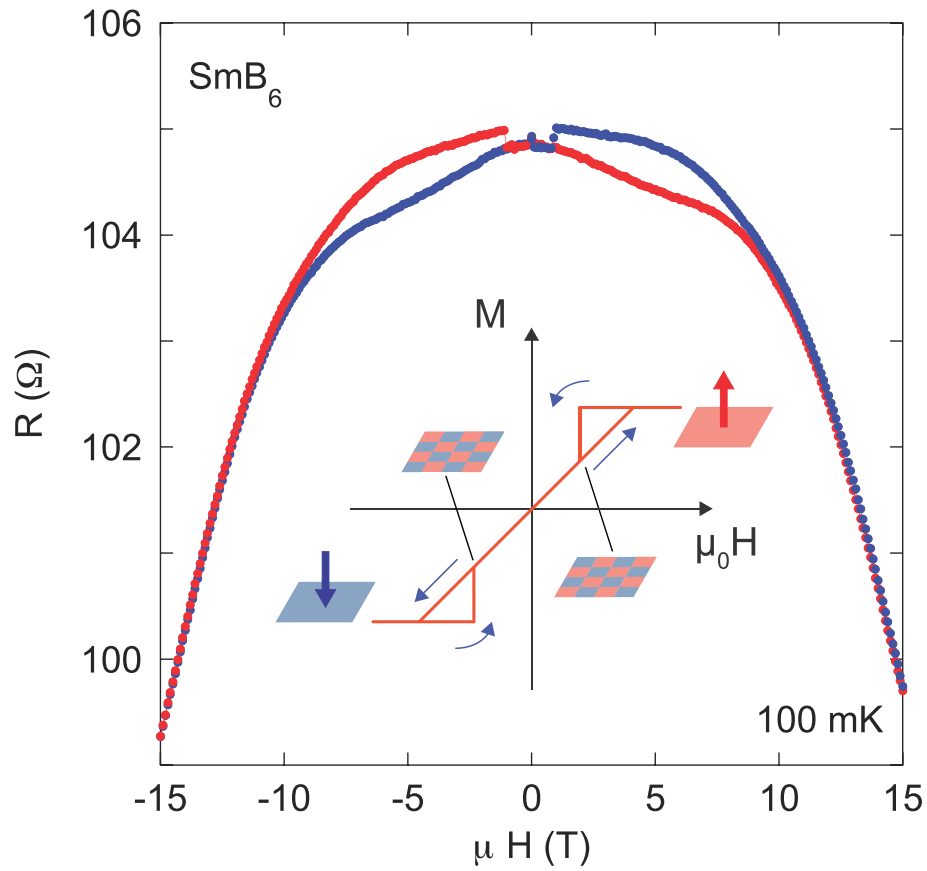


Figure S4: **Off-centered hysteresis and schematic magnetization.** Full “four quadrant” magnetoresistance hysteresis loop of sample #1 in field perpendicular orientation ($I \parallel [100]$, $H \parallel [001]$) measured at 100 mK. The inset presents a schematic of the magnetization hysteresis curve of an exchange bias system (see text).

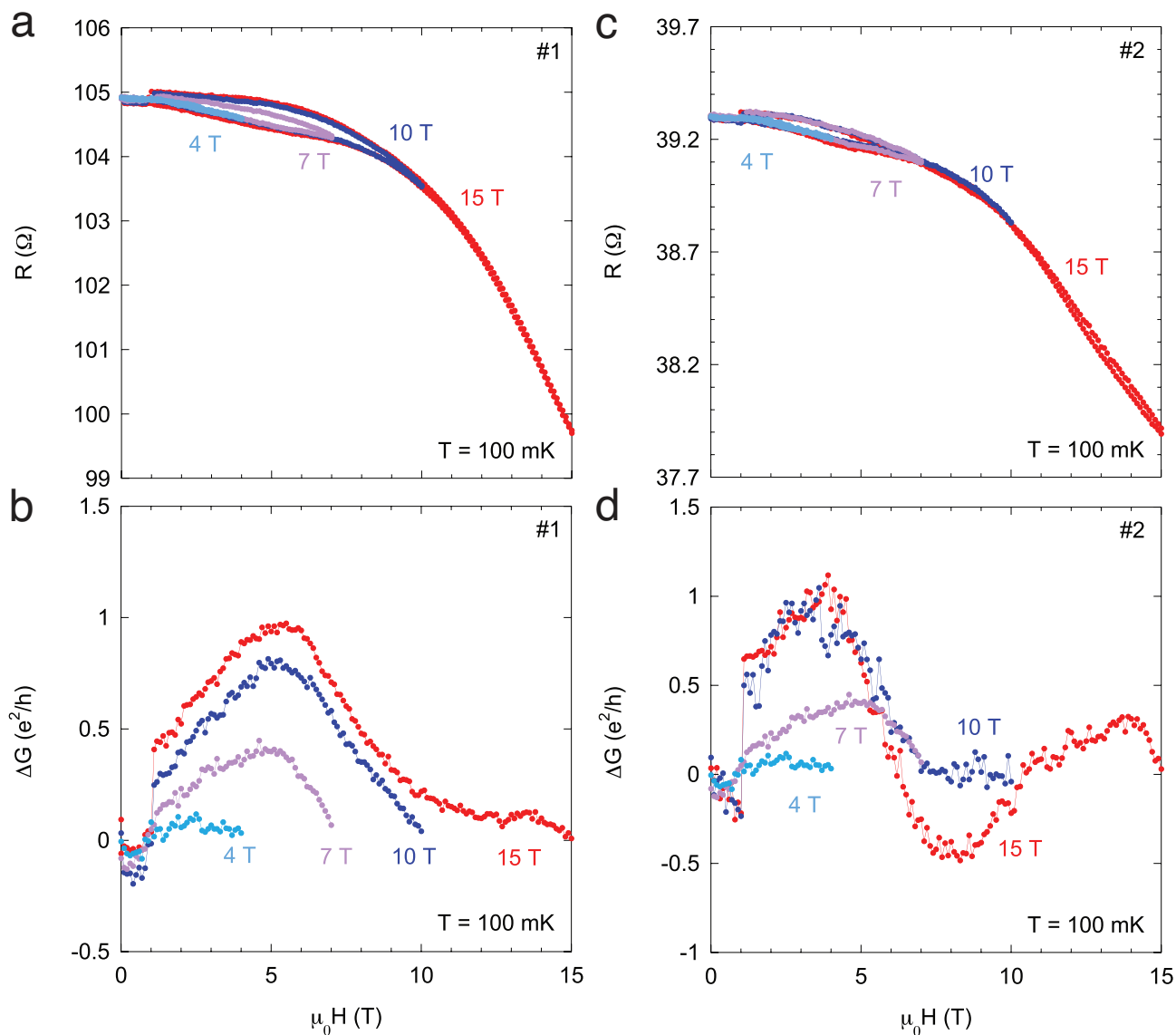


Figure S5: **Hysteresis in magnetoresistance and magnetoconductance with different turning fields.** **a, b**, Hysteresis loop in field perpendicular orientation ($I \parallel [100]$, $H \parallel [001]$) for sample #1 and #2 at 100 mK with different turning fields. The hysteresis loop shrinks with decreasing turning field, and disappears below 4 T. **c, d**, Difference between sweep-up and sweep-down magnetoconductance $\Delta G = G_{up} - G_{down}$ obtained from the data shown Figs. S4a and b. The peak of ΔG is suppressed with decreasing turning fields.

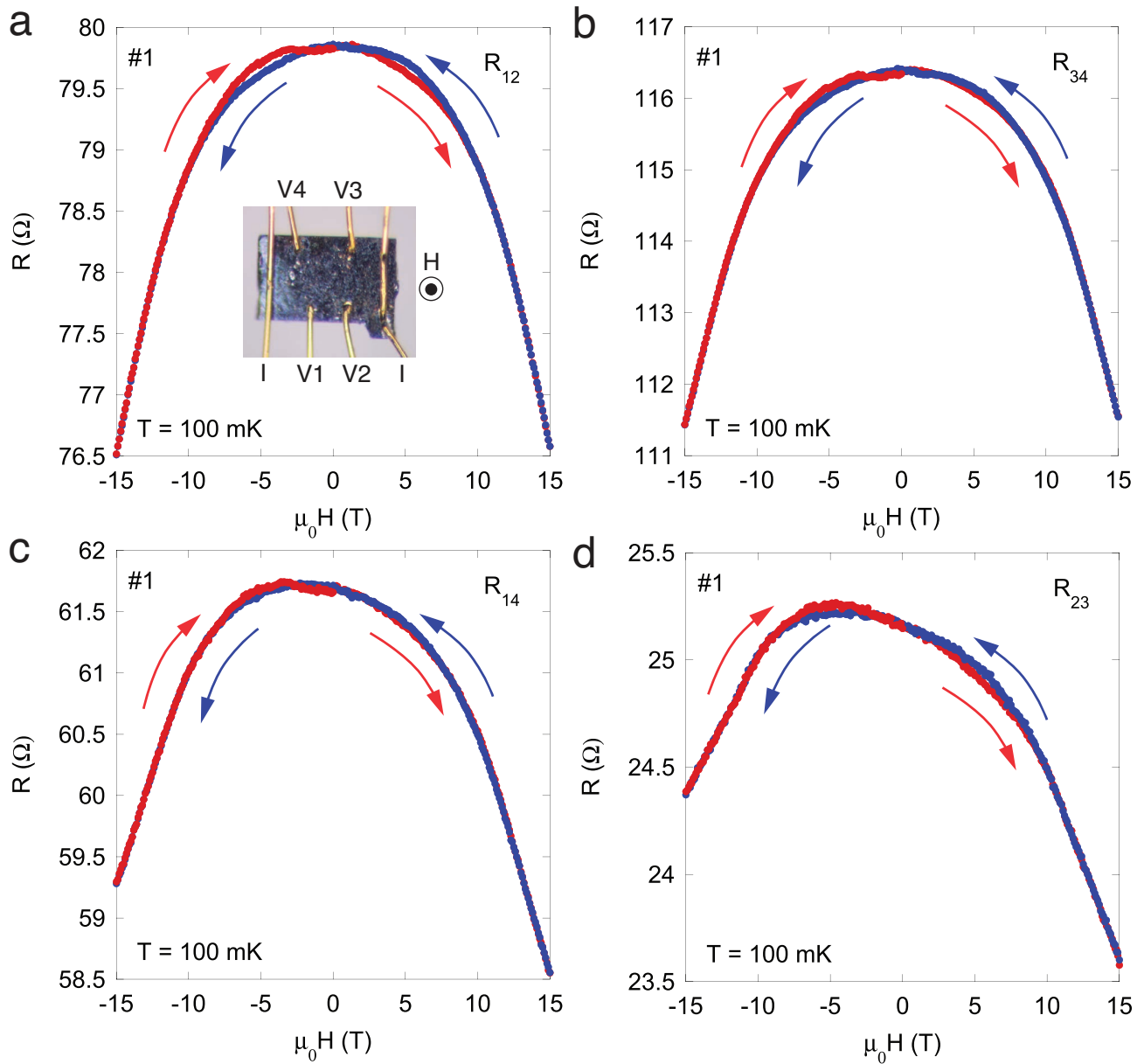


Figure S6: Longitudinal and transverse resistance for sample #1 as a function of magnetic field at 100 mK. Field dependence of longitudinal resistance R_{12} a, between voltage probes V1 and V2, and b, R_{34} between V3 and V4 shown in the inset. Contacts were applied with spot welding. Field dependence of transverse resistance R_{14} c, between V1 and V4, and d, R_{23} between V2 and V3.

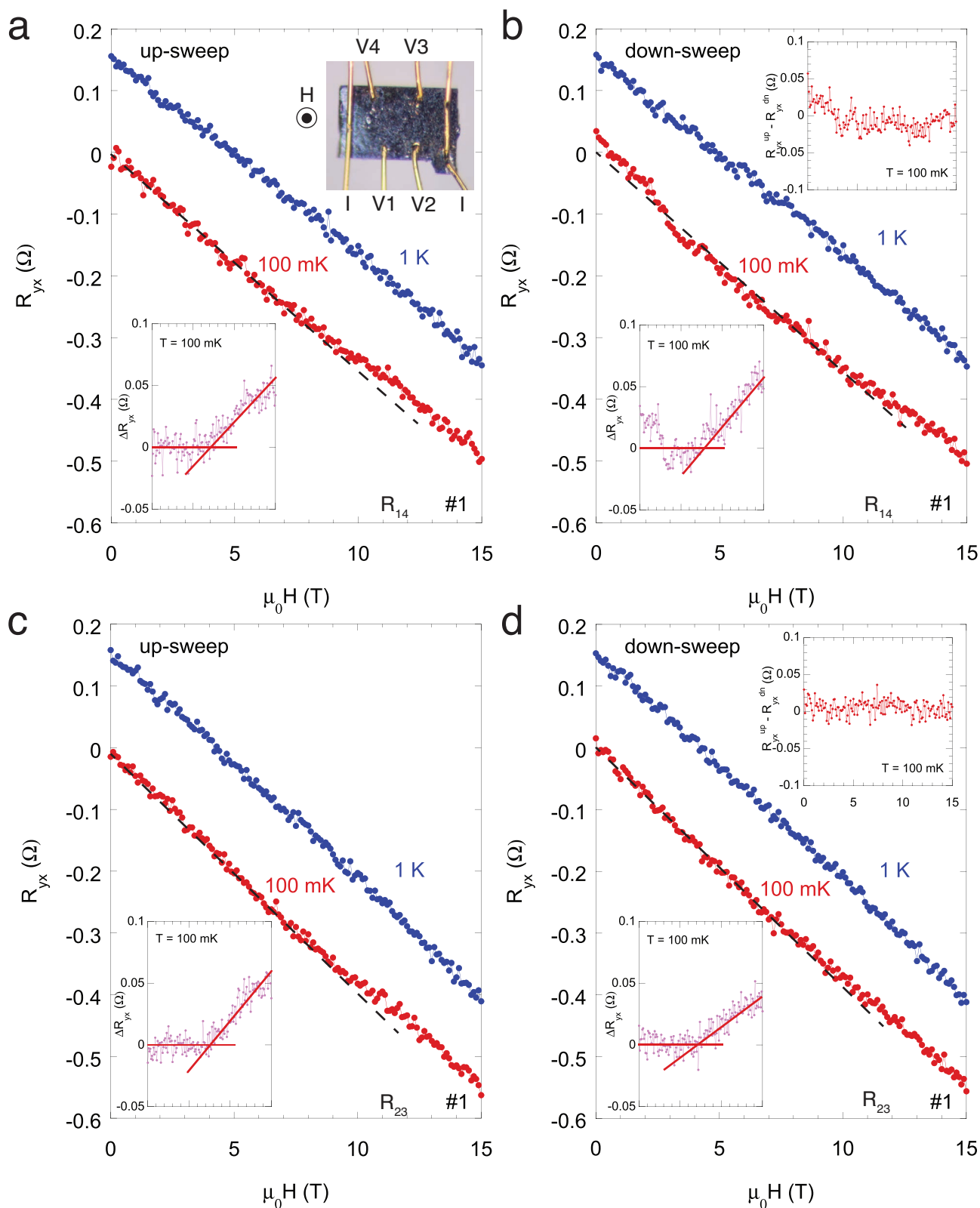


Figure S7: **Anomalous Hall effect.** **a**, up-sweep and **b**, down-sweep Hall resistance R_{yx} for sample #1 at 100 mK and 1K, obtained from transverse resistance R_{14} between V1 and V4 using eqs. (S1) and (S2). Contacts were applied with spot welding. **c**, up-sweep and **d**, down-sweep Hall resistance R_{yx} for sample #1 at 100 mK and 1K, obtained from transverse resistance R_{23} between V2 and V3. Lower insets show the difference of the Hall resistance $\Delta R_{yx} = R_{yx} - AH$ at 100 mK, where A is a linear coefficient obtained from fitting R_{yx} below 5 T. Upper insets of **b** and **d** show the difference between R_{yx}^{up} and R_{yx}^{dn} at 100 mK, indicating indiscernible hysteresis in the Hall resistance, in spite of the presence of prominent hysteresis in longitudinal resistance (see text).

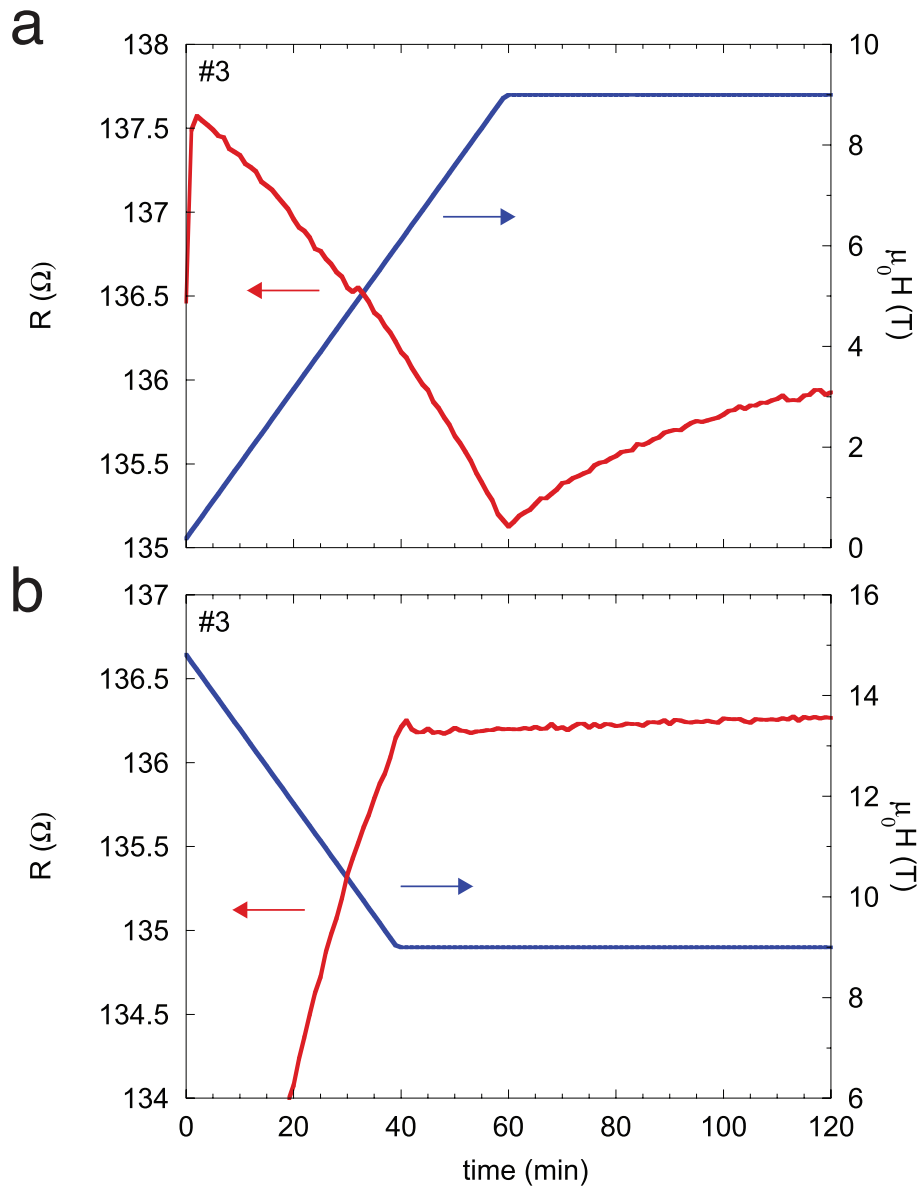


Figure S8: **Asymmetric relaxation of magnetoresistance.** Relaxation at 9 T in **a**, ascending and **b** descending field sweeps at 30 mK for SmB_6 sample #3 (spot-welded). The relaxation of magnetoresistance in ascending field sweep is much slower than that in descending one, which strongly indicates the presence of magnetic domains.

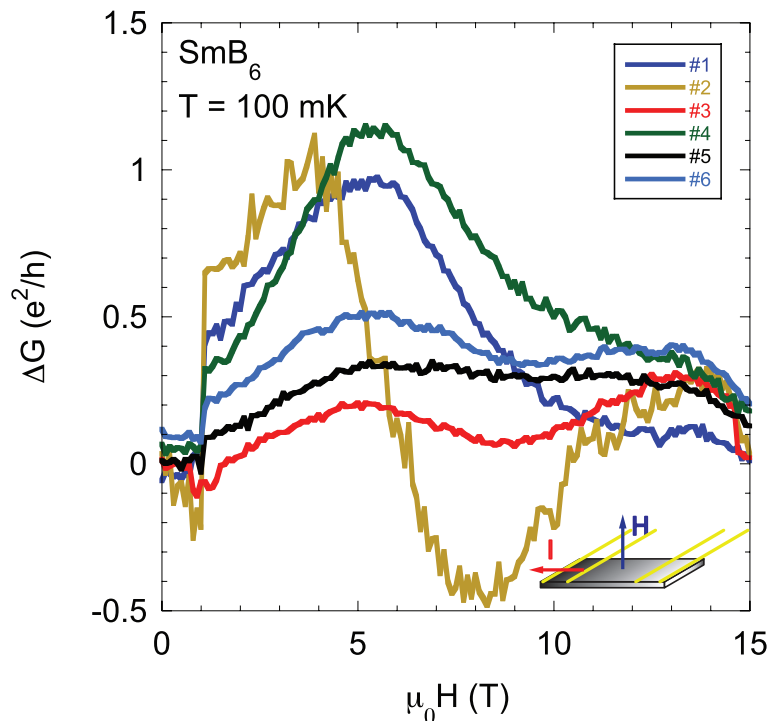


Figure S9: **Nearly quantized magnetoconductance in various samples.** Field dependence of difference of sweep-up and sweep-down $\Delta G = G_{up} - G_{down}$ in field perpendicular orientation ($I \parallel [100]$, $H \parallel [001]$) for various samples at 100 mK. The peak of ΔG reaches order of e^2/h , attributed to a grid-shape ferromagnetic domain structure (see text).

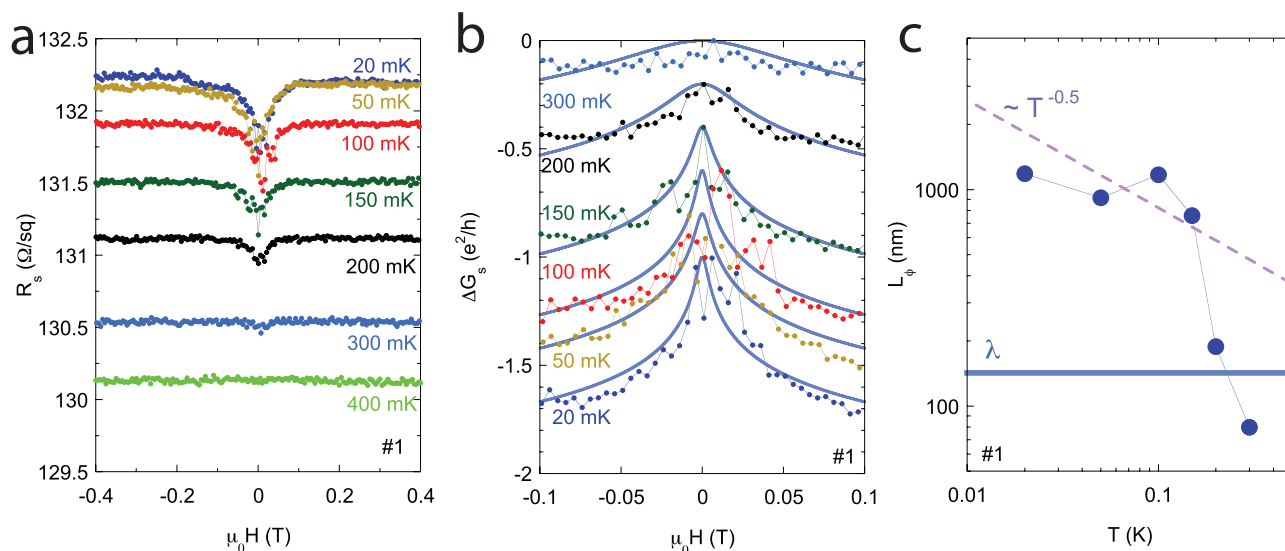


Figure S10: **Weak antilocalization in low field magnetoresistance of SmB_6 .** **a**, Field dependence of sheet resistance R_s estimated from the top surface in parallel field orientation ($I \parallel [100]$, $H \parallel [010]$) for sample #1. **b**, In-plane WAL fit to the magnetoconductance with $\alpha = 0.29$ and the penetration depth $\lambda = 142$ nm (see text). Each curve is offset by $0.2e^2/h$. **c**, Temperature dependence of dephasing length L_ϕ . The dephasing length varies as $L_\phi \sim T^{-0.5}$ (dashed line) at low temperatures, but starts deviating from the $T^{-0.5}$ dependence as approaching the penetration depth λ , indicating the finite penetration depth approximation is not valid at high temperatures.

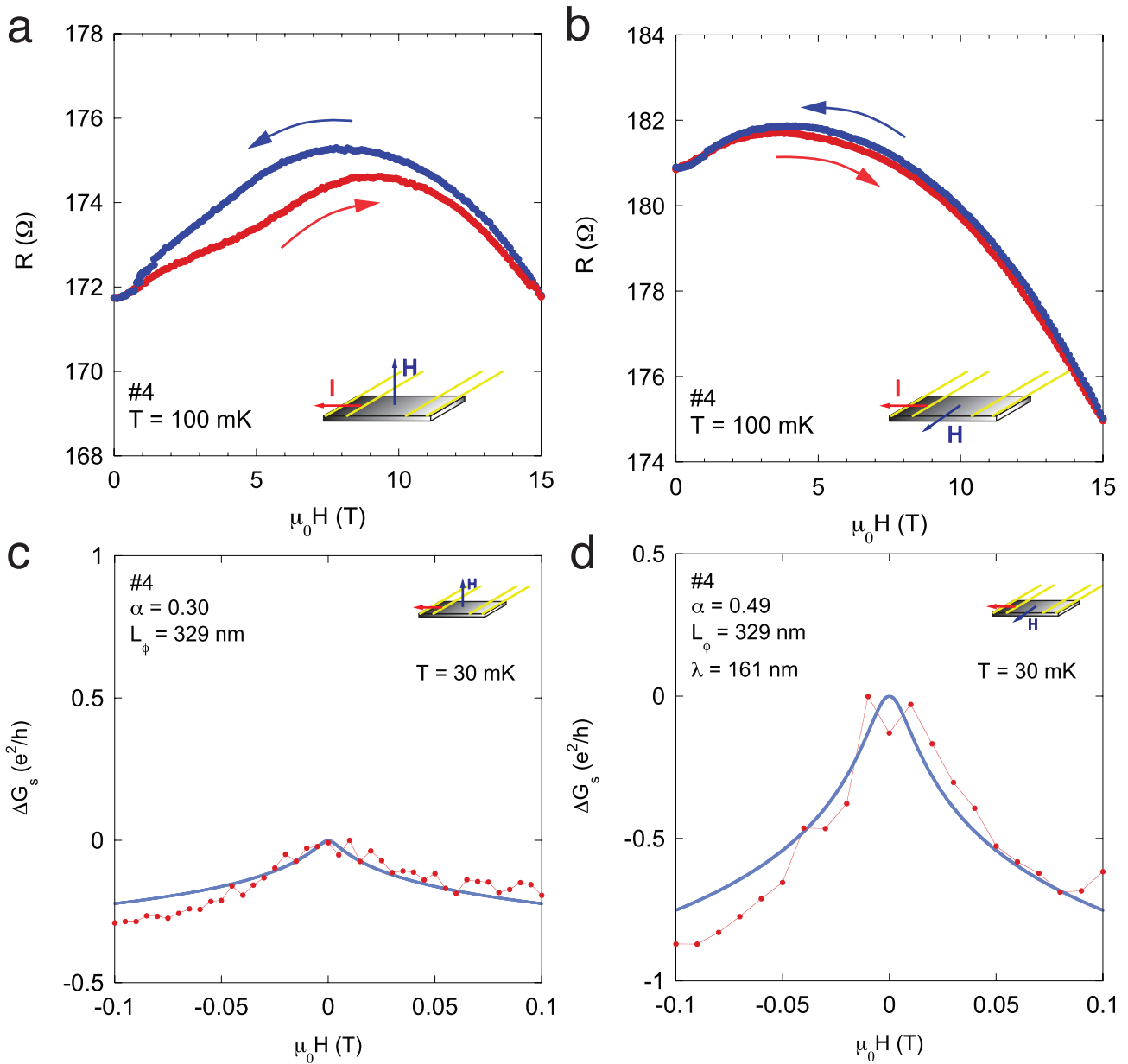


Figure S11: **Positive magnetoresistance with hysteresis and weak antilocalization.** **a**, Magnetoresistance in perpendicular field and **b** in parallel field to conduction surface for SmB₆ sample #4. Positive magnetoresistance and hysteresis are suppressed in parallel field orientation. **d**, **e**, Weak antilocalization fit for sample #4 without reapplying electrical contacts (spot-welded), showing strong anisotropy similar to sample #1. Obtained $\alpha_\perp=0.30$ for perpendicular and $\alpha_\parallel=0.49$ for parallel field orientation are different from that of #1, but the penetration depth λ is comparable (see text).